Chemical Methodologies 9(2025) 643-661

Chemical Methodologies

Journal homepage: http://chemmethod.com

Original Article

Theoretical Study of the Effect of Phase Transition on the Structural and Electronic Properties of Lanthanide-Doped Chromium Chalcogenide Monolayers

Murtagi Kadhim Jwaid Almuttwaki, Mahmood Rezaee Roknabadi*, Mohsen Modarresi

Department of Physics, Faculty of Science, Ferdowsi University of Mashhad, Mashhad, Iran

ARTICLEINFO

Article history

Submitted: 2025-02-17
Revised: 2025-04-11
Accepted: 2025-04-27
ID: CHEMM-2502-1905

DOI: 10.48309/CHEMM.2025.506714.1905

KEYWORDS

Density functional theory
Quantum ESPRESSO
Chromium chalcogenides
Lanthanide atom
Band structure spintronic devices

ABSTRACT

This study investigates the structural and electronic properties of octahedral and hexagonal phases of CrX_2 monolayers (where X = S, Se) using the Quantum ESPRESSO package. Employing a first-principles density functional theory (DFT) approach with generalized gradient approximation (GGA), we analyze the impact of lanthanide atoms (L = Ce, Pr, and Nd) on the structural and electronic features of CrX_2. Total energy, bond length, bond angle, and curvature are examined both with and without lanthanide atoms. The primitive unit cell of the 2H/1T phase forms a 120° rhombus with space groups (P63/mmc)/(P31). Structural analysis demonstrates a direct correlation between atomic number and geometrical properties, where increasing lanthanide atomic number leads to longer Cr-X and L-X bond lengths, alongside the smaller X-Cr-X and X-L-X bond angles. A comparison of total energy between hexagonal and octahedral phases indicates that the latter exhibits greater stability. The band structure of CrX_2 (where X = S, Se) monolayers is studied both with and without lanthanide atoms, concerning spin effects. The results show that the octahedral phase of CrX_2 exhibits metallic behavior with multiple bands intersecting the Fermi level, while the hexagonal phase displays semiconducting behavior with band gap values of 0.30 eV and 0.44 eV, respectively. Concerning spin polarization in the presence of lanthanide atoms, CrX_2 demonstrates half-metal behavior, suggesting its suitability for use in spintronic components.

* Corresponding author: M.R. Roknabadi
E-mail: roknabad@um.ac.ir

GRAPHICALABSTRACT

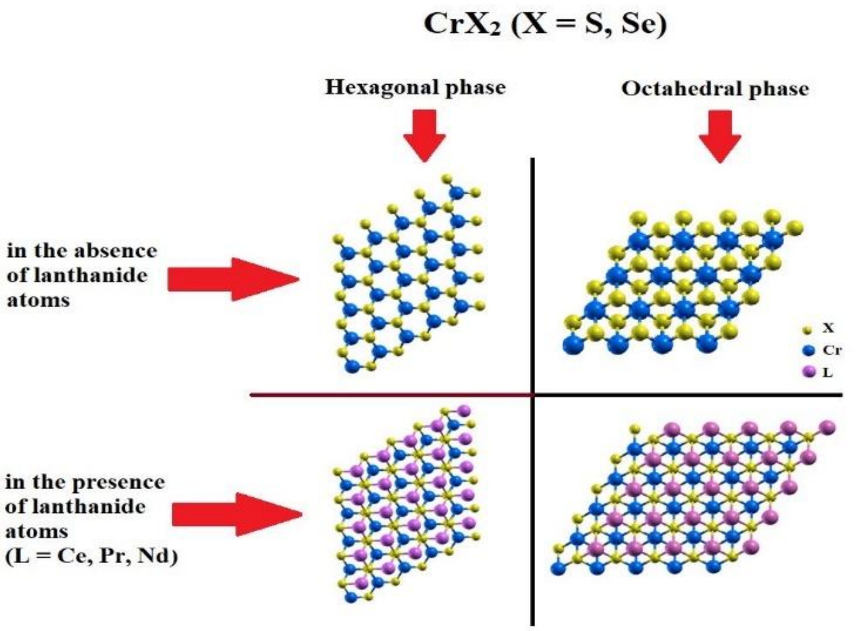

Introduction

Two-dimensional (2D) materials, characterized by their smaller dimensions and quantum confinement effect, exhibit unusual properties, and offer potential for diverse applications compared to bulk structures. Rapidly expanding 2D materials such as graphene, black phosphorene, borophene, silicene, and transition metal dichalcogenides (TMDs) have attracted considerable interest in scientific and engineering domains. TMDs, characterized by the MX_2 formula (where, M represents a transition metal atom from groups IV-VIII and X denotes a atom including S, Se, or Te), are the prominent representatives of 2D materials due to their diverse crystal structures and ultra-thin thickness, leading to novel applications in electronics, optoelectronics, catalysts, energy storage, among others [1-8].

The two principal phases of 2D compounds with the MX_2 chemical formula are the 2H and 1T phases, featuring a triangular prism and octahedral structure, respectively [1]. The physical properties of MX_2 monolayers are strongly linked to their crystal structure and electronic band structure. In the following, several research studies related to these materials will be introduced.

In a study conducted by H. Y. Lv *et al.* [2], the magnetic properties of $CrSe_2$/$CrTe_2$ monolayers under in-plane biaxial compression and tension were investigated. The findings revealed that under no strain, $CrSe_2$ and $CrTe_2$ monolayers exhibit antiferromagnetic (AFM) and ferromagnetic (FM) behavior, respectively, consistent with their bulk counterparts. Interestingly, strain emerged as an effective means to modulate the magnetic and electronic properties of $CrSe_2$/$CrTe_2$ monolayers, positioning them as potential candidates for future nano-electronic applications warranting further experimental investigation.

In the research conducted by Kaiyun Chen *et al.* [9], using density functional theory (DFT) calculations, all TMDs from groups IV, V, and VI were systematically studied. The study introduced CrS_2 as a unique material suitable for spintronic device design, offering diverse electronic and magnetic properties to meet the demands of spintronic systems. CrS_2 exhibits a non-magnetic semiconductor 2H phase with a direct band gap and an antiferromagnetic metallic 1T phase. Notably, its 1T' phase represents the ferromagnetic ground state and serves as a semiconductor with indirect band gaps of 0.26 eV and 1.92 eV for up-spin and down-spin electrons, respectively. Remarkably, uniaxial compression and tension along the y-direction can transform the 1T phase into either an up-spin or down-spin semi-metallic state, presenting a unique feature beneficial for spintronic device design. The findings underscore CrS_2 as an excellent material for developing simple and cost-effective structures for producing multifunctional spintronic nanoscale devices. In the review article published by Maria Hasan *et al.* [10], Crystal structure, synthesis, and characterization of different chromium-based two-dimensional compounds were studied comprehensive. This review article indicates that 2D chromium-based compounds synthesized through CVD could contribute majorly to the emerging field of spintronics circuits.

Researchers [11] investigated the stability and electronic properties of MX_2 monolayers using density functional theory (DFT) simulations. Moreover, the absorption and diffusion of lithium in the stable phase of MX_2 were explored. The results indicate that lithium is energetically adsorbed on MX_2 monolayers, which exhibit narrow bandgap semiconductor or metallic behavior. These findings suggest that most MX_2 monolayers hold promise as potential anode materials for Li-ion batteries. In the report by Bastos *et al.* [12], investigations were conducted on 27 compositions of bulk transition metal dichalcogenides (TMDs), combining 9 transition metals (Ti, Zr, Hf, V, Nb, Ta, Cr, Mo, and W) with three chalcogens (S, Se, and Te) across three phases: 1T, 2H, and 1Td. Equilibrium geometry configurations and the lowest energy phase for each material were calculated, corresponding with experimental data for previously synthesized compounds. Magnetic order was also considered, revealing that certain compounds containing Cr and transition metals in the V group exhibit ferromagnetic or antiferromagnetic behavior. The exfoliation energy of all stable materials was determined, indicating weak interlayer coupling for most studied TMDs, implying that their 2D form can be easily synthesized through the exfoliation method.

Wang *et al.* [13] demonstrated the tunability of intralayer magnetization in CrS_2 multilayers through interlayer engineering, direct charge doping, and elemental substitution. Notably, the transition from spin-antiferromagnetic (sAFM) to in-plane ferromagnetic (FM) occurs as thickness increases from monolayer to multilayer, with interlayer coupling strongly favoring FM. Their results underscore the exceptional tunability of magnetic properties alongside electronic, mechanical, vibrational, and optical properties, opening avenues for manipulating CrS_2 multilayers transitioning between sAFM and FM modes for applications in magnetic data recording and processing.

In a study published by Korotaev *et al.*, the effect of adding lanthanides on chromium chalcogenide was investigated, revealing that while states distribution, it does increase phonon scattering and decrease the thermal conductivity of these materials [14].

In general, the previous studies demonstrate that TMDs exhibit interesting band structures with tunable band gaps, a crucial element determining their properties and applications in various fields. Unlike graphene, which is a semi-metal with a zero-band gap limiting its applications in electronics and photoelectronics [15-21], TMDs offer variable band gaps ranging from zero to 3 eV, tunable by factors such as thickness, defects, impurities, and mechanical deformation (compression and tension). Leveraging their unique crystal and electronic structures, TMDs hold immense potential across electronics, optoelectronics, catalysis, energy conversion and storage, and sensing applications [22-28].

Studies have been conducted by researchers to investigate the structural and electronic properties of lanthanide-doped TMDs. For example, Effects of La and Ce doping on electronic structure and optical properties of janus MoSSe monolayer reported by Thi-Nga Do *et al.* [29]. Their results show that by increasing the doping concentration, Janus MoSSe monolayer switched from semiconductor to metal. Likewise, they report that La and Ce doped MoSSe monolayer are potential candidate for spintronics, nanoelectronics, and optoelectronics. Experimental fabrication and computational investigations of La-Doped MoS_2 nanosheets with tuned bandgap for dye degradation and antimicrobial activities reported by Muhammad Ikram *et al.* [30]. A redshift is observed upon La doping, indicating that the bandgap is lowered after La doping in MoS_2. Investigation of the changes in bandgap and electronic structure reveal that doping of La introduces new states within the bandgap region, allowing for further induced energy transitions. JIANG Gange *et al.* [31] studied the structure, as well as electrical and optical properties of rare earth element (La, Eu, and Ho) doped monolayer WSe_2 based on DFT. Monolayer tungsten selenide possesses outstanding properties, including the excellent thermal stability, electronic transport, and large-scale scalability. Doping with rare earth elements (La, Eu, and Ho) results in a P-type conductive transmission characteristic of monolayer WSe_2, enhancing its conductivity and exhibiting semi-metallic properties. In addition, doping with La, Eu, and Ho improves the light detection ability and visible light utilization of monolayer WSe_2 in the infrared region, and has potential applications in the deep ultraviolet region.

To the best of our knowledge, among the extensive research on TMDs, there are no first-principle studies on the effect of adding lanthanides on the structural and electronic properties of chromium chalcogenide (CrX_2) monolayers. Therefore, this research aims to theoretically investigate the structural and electronic properties of different phases of CrX_2 (X=S, Se) monolayers in the presence of lanthanides (Ce, Pr, and Nd).

Computational Method

All calculations in this research were conducted using the Quantum Espresso computing package based on density functional theory (DFT) [32]. The generalized gradient approximation GGA-PBE was selected for the exchange-correlation potential [33]. The norm-conserving pseudopotentials were used for Cr, S and Se atoms. Density functional theory calculations were performed for a specific set of k points within the first Brillouin zone using a self-consistent method. The accurate selection of parameters such as the number of k points and the convergence parameter significantly impacts the speed and accuracy of the calculations. As depicted in Figure 1, the appropriate cutoff energy to distinguish valence states and core states of CrS_2-2H, CrS_2-1T, $CrSe_2$-2H, $CrSe_2$-1T monolayers was determined to be 200, 100, 100, and 200 Ry, respectively. Using these energy values, the entire structure under consideration was minimized. The suitable number of k points to achieve sufficient accuracy and minimize the total energy was selected as (20×20×1), (24×24×1), (30×30×1), and (22×22×1) for CrS_2-2H, CrS_2-1T, $CrSe_2$-2H, and $CrSe_2$-1T monolayers, respectively, based on Figure 2. To prevent the interaction between the adjacent layers, a vacuum layer of 20 Å was included perpendicular to the plane of the structures. Subsequently, all studied structures in the presence and absence of lanthanide atoms were optimized by minimizing the pressure and force up to the order of 10^{-6}. Van der Waals interaction correction is not considered in this study. The spin–orbit coupling (SOC) effect is not considered because the SOC effect on band structure is negligible for CrS_2, as reported in previous study [9,34].

Results and Discussion

Crystal Structure of CrX_2 Monolayers in the Presence and Absence of Lanthanides

The physical properties of CrX_2 monolayers are closely related to their crystal and electronic structures, necessitating a thorough understanding of their crystal structures. CrX_2 monolayers exhibit three phases: hexagonal (2H), octahedral (1T), and distorted octahedral (1T'). For this study, we focused on the two most stable phases: 2H and 1T. Figures 3 and 4 illustrate the geometrical structures of the hexagonal (2H) and octahedral (1T) phases of chromium chalcogenide (CrX_2, where X=S, Se) monolayers after relaxation, from side view (a) and top view (b), respectively. Ball-and-stick models of the hexagonal and octahedral phases of the structures in the presence of lanthanides (Ce, Pr, and Nd) are shown in Figures 5 and 6, respectively. The primitive unit cell is a 120° rhombus with a P63/mmc space group for the 2H phase and a P31 space group for the 1T phase. The 2H phase can transition to the 1T phase by sliding the top layer (X atoms) to the hexagon centers [11]. Several stimuli such as heat, electrochemical doping, and strain can convert the 2H phase to the 1T phase [35]. Qiu Jin *et al.* [36] discussed various 2H→1T phase transition mechanisms of MoS_2 nanosheets that consist of nucleation and propagation steps, which were simulated by collective rotational and rotational/translational movements, single atom translational movement, and the gliding movement of one row for sulfur (S) atoms, on both the basal plane and Mo- and S-edges with different S coverages were investigated.

The crystal structure consists of a 2D layer of Cr atoms (positively charged) sandwiched between two hexagonal lattices of X atoms (negatively charged). Each Cr atom is surrounded by the six nearest chalcogen atoms, and each X atom is linked to the three nearest Cr atoms with ionic Cr–X bonds. The Cr atoms are located at the lattice positions of hexagonal close-packed/octahedral centers in the 2H/1T phase [11]. In the pure structure of these samples, the unit cell comprises three atoms (two X atoms and one Cr atom), and the bond lengths between the atoms are provided in Table 1 compared with the results of other researchers. Based on Table 1, it is evident that the structural properties of CrX_2 monolayers obtained in this study align with the findings of other researchers [11-13]. With lanthanides, a lanthanide atom is introduced at the top of the structure, indicated in pink in Figures 5 and 6. Therefore, the unit cell of lanthanide-doped structures consists of four atoms: one chromium atom, two chalcogen atoms, and one lanthanide atom. Table 1 indicates the total energy of the structures after relaxation, curvature value, bond angle, and lattice constant. The total energy encompasses the kinetic energy of the non-interacting system, external energy, Hartree energy, and exchange-correlation term. Examination of the results reveals that the total energy of the CrS_2 structure is more negative than that of the $CrSe_2$ structure, indicating the greater stability of CrS_2 in terms of energy. In addition, a slight energy difference exists between the hexagonal and octahedral phases, with the octahedral phase exhibiting a higher stability. This finding is consistent with previous research, which confirms the 1T phase is more stable than 2H in CrS_2 [11] and $CrSe_2$ [12]. With lanthanides, the stability of the structures increases compared to their pure state, reflected by a more negative total energy. Furthermore, increasing the atomic number of lanthanides doped into the structure results in more negative total energy and increased structural stability. Cr-X bond length and X-Cr-X bond angle are larger in the hexagonal phase compared to the octahedral phase. With lanthanides, the Cr-X bond length increases, with the longest bond length observed for the Nd atom and the shortest for the Ce atom. Moreover, increasing the atomic number of lanthanides leads to longer Cr-X and L-X bond lengths and decreased X-Cr-X and X-L-X bond angles. The results analysis indicates a direct relationship between atomic number and bond length. Generally, the bond length between two atoms is the sum of their covalent radii, with larger atomic numbers corresponding to larger covalent radii and consequently longer bond lengths. Other reports also demonstrate an increase in lattice constants and bond lengths across all MX_2 (in this study M=Cr) monolayers as the element X varies from S to Te [11]. This variation can be attributed to the increasing atomic radius of elements X from S to Te. Curvature is the buckling parameter which was calculated using XCrySDen software. Concerning curvature, the hexagonal phase exhibits more bending compared to the octahedral phase, and the presence of lanthanides enhances the curvature, as expected.

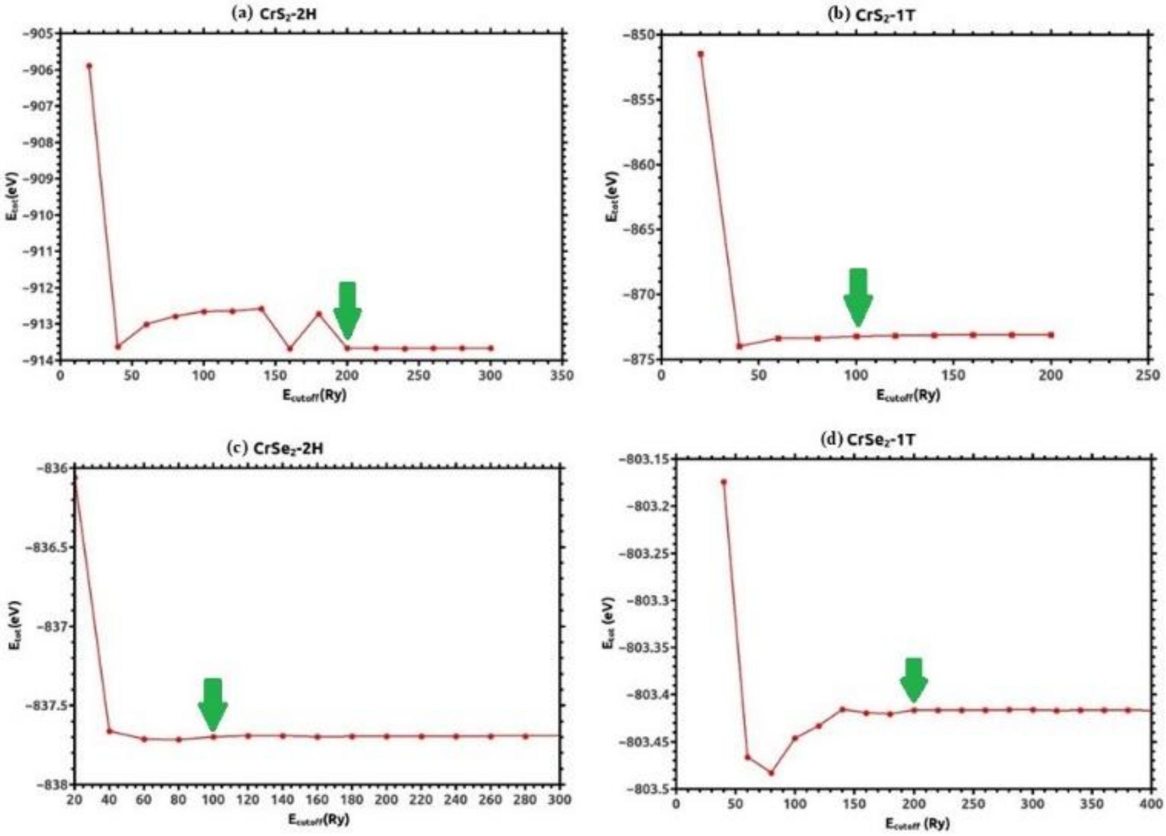

Figure 1: Variation of total energy (eV) in terms of the cutoff energy (Ry) of (a) CrS_2-2H, (b) CrS_2-1T, and (c) $CrSe_2$-2H and (d) $CrSe_2$-1T structures. Green arrow indicates proper cutoff energy

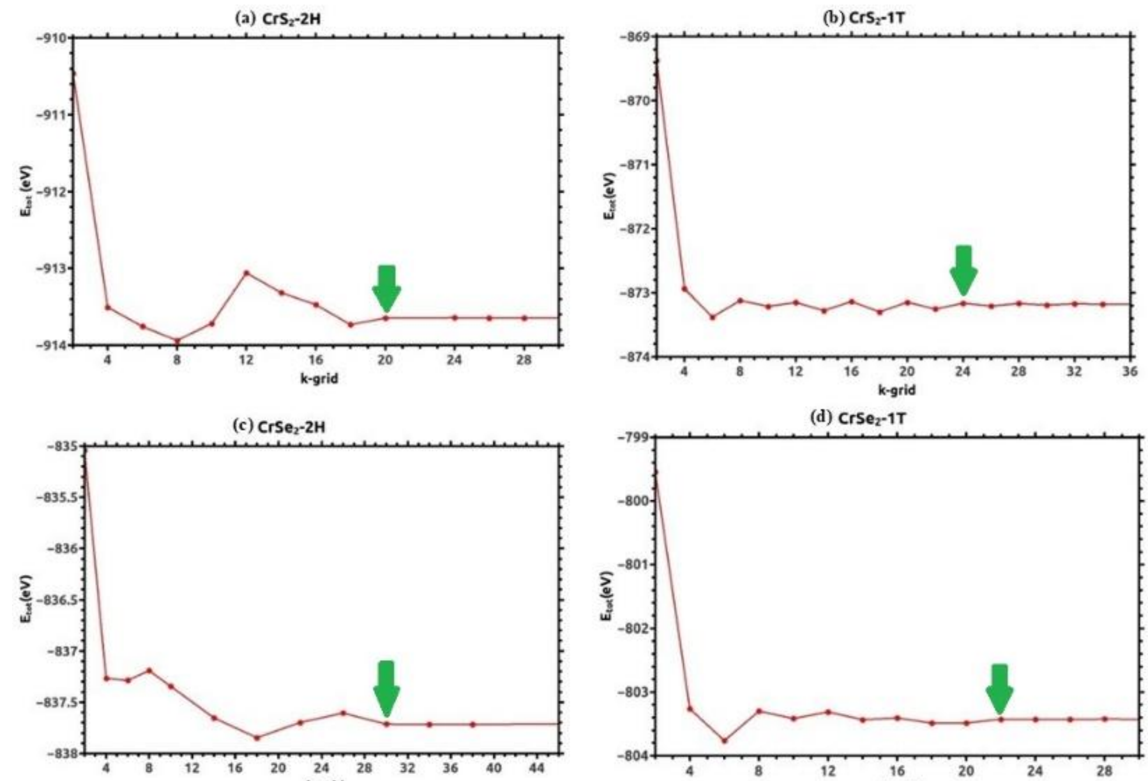

Figure 2: Variation of total energy (eV) in terms of k-grid of (a) CrS_2-2H, (b) CrS_2-1T, (c) $CrSe_2$-2H, and (d) $CrSe_2$-1T structures. Green arrow indicates proper k-grid

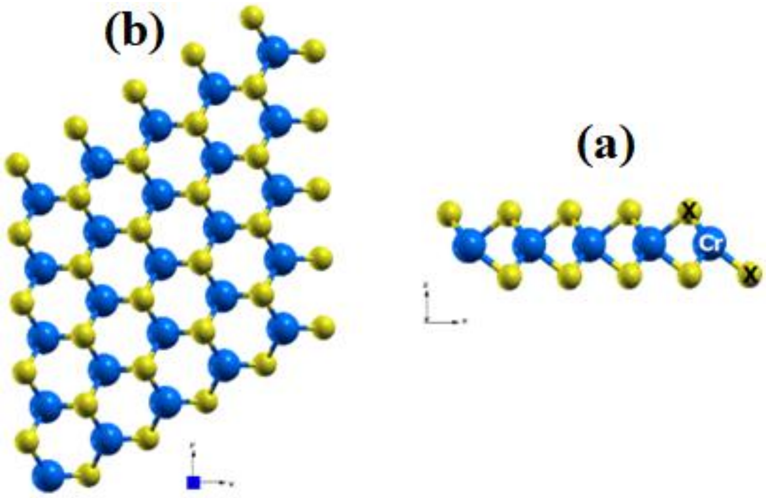

Figure 3: Geometrical structure of hexagonal phase of CrX_2 (where X = S, Se) monolayers after relaxation from side view (a) and top view (b). Chromium atom is marked with blue color and chalcogen atom is marked with yellow color

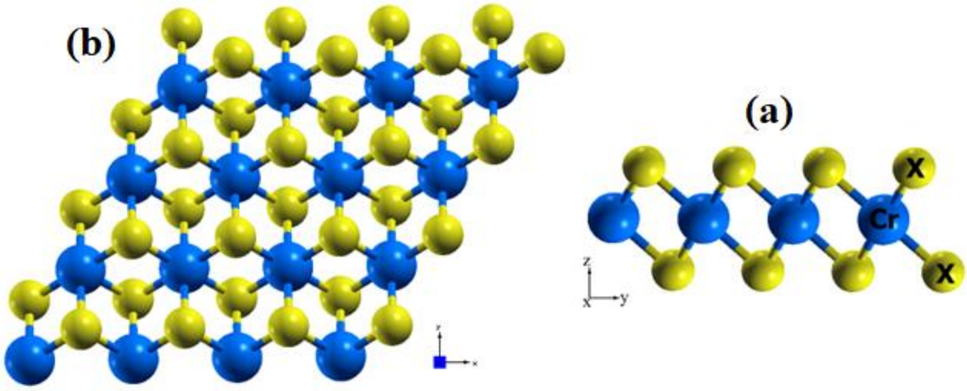

Figure 4: Geometrical structure of octahedral phase of CrX_2 (where X = S, Se) monolayers after relaxation from side view (a) and top view (b). Chromium atom is marked with blue color and chalcogen atom is marked with yellow color

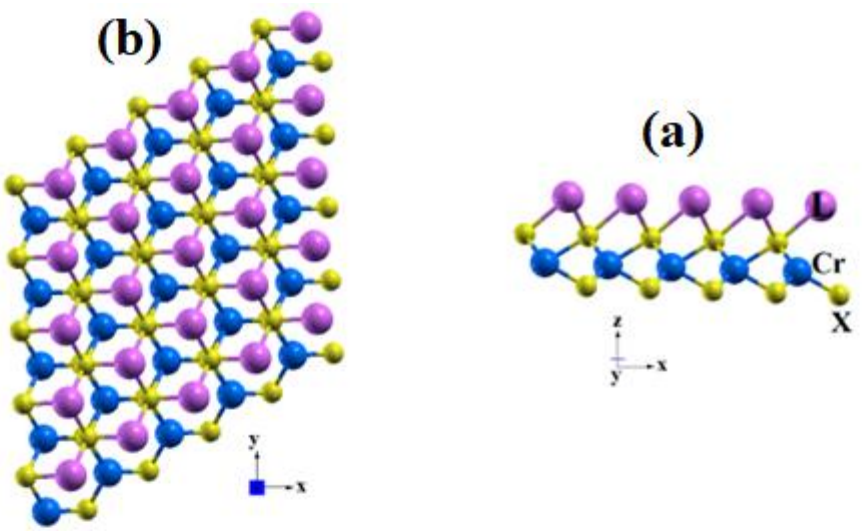

Figure 5: Geometrical structure of the hexagonal phase of CrX_2 (where X = S, Se) monolayers with lanthanide atoms (L = Ce, Pr, and Nd) after relaxation from side view (a) and top view (b). Chromium atom is marked with blue color, chalcogen atom with yellow color, and lanthanide atom with pink color

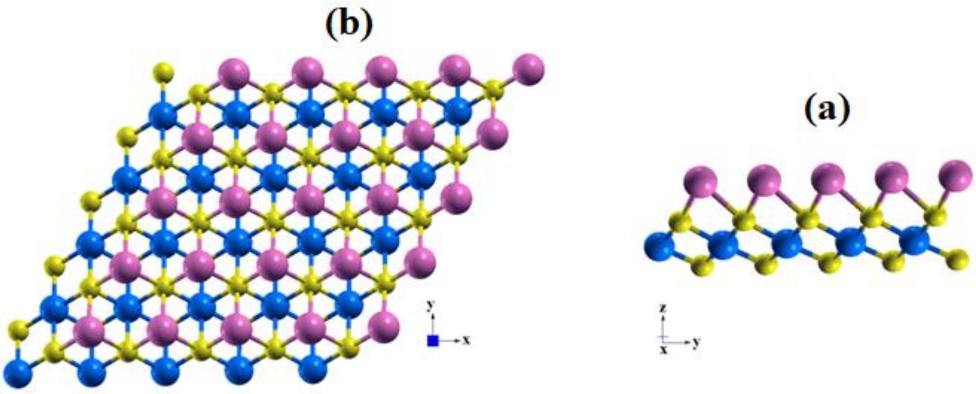

Figure 6: Geometrical structure of the octahedral phase of CrX_2 (where X = S, Se) monolayers in the presence of lanthanide atoms (L = Ce, Pr, and Nd) after relaxation from side view (a) and top view (b). Chromium atom is marked with blue color, chalcogen atom with yellow color, and lanthanide atom with pink color

Table 1: Total energy, bond length, curvature value, and bond angle of hexagonal (2H) and octahedral (1T) phase of CrX_2 (where X=S, Se) structures after relaxation with and without lanthanide atoms (L=Ce, Pr, and Nd) and comparison with the previous results

Structure		Total energy (eV)	Cr-X Bond length (Å)	L-X Bond length (Å)	curvature (Å)	X-Cr-X Bond angle (°)	L-X-L Bond angle (°)
CrS_2 - 2H	pure	-915.45	2.42 2.318[41]	–	4.44	133.75	–
	+Ce	-1023.95	2.75	3.06	4.83	100.43	79.79
	+Pr	-1094.45	2.78	3.07	4.84	100.19	79.36
	+Nd	-1162.88	2.83	3.09	4.88	100.02	79.14
CrS_2 - 1T	pure	-915.89	2.40 2.41 [11] 2.38 [13]	–	2.87	91.21 88.2 [12]	–
	+Ce	-1024.77	2.61	3.06	4.34	83.94	80.14
	+Pr	-1095.35	2.64	3.09	4.42	83.29	79.37
	+Nd	-1163.60	2.66	3.10	4.45	82.89	79.11
$CrSe_2$ - 2H	pure	-837.48	2.57 2.452[41]	–	4.74	134.15	–
	+Ce	-947.07	2.77	3.21	5.13	100.29	79.99
	+Pr	-1017.65	2.86	3.22	5.17	99.80	79.74
	+Nd	-1085.89	2.88	3.26	5.24	99.09	79.27
$CrSe_2$ - 1T	pure	-838.04	2.45 2.56 [11]	–	3.21	98.04	–
	+Ce	947.87–	2.72	3.23	4.68	82.02	78.45
	+Pr	-1018.32	2.74	3.24	4.71	81.75	78.36
	+Nd	-1086.42	2.76	3.27	4.75	81.13	77.99

Band Structure of CrX_2 Monolayers with and without Lanthanide Atoms without Spin Polarization Effect

The band structure reveals the permitted energy levels that electrons can adopt with the k wave vector. It determines the conductivity characteristics of the material (*i.e.* conductor, semiconductor, and insulator), as well as the location and size of the energy gap and the Fermi level value. Directions with high symmetry in the first Brillouin zone are chosen along the K-Γ-M-K path. The band structure of CrS_2-2H, CrS_2-1T, $CrSe_2$-2H, and $CrSe_2$-1T monolayers in the presence and absence of lanthanide atoms (L = Ce, Pr, and Nd) is depicted in Figures 7-10.

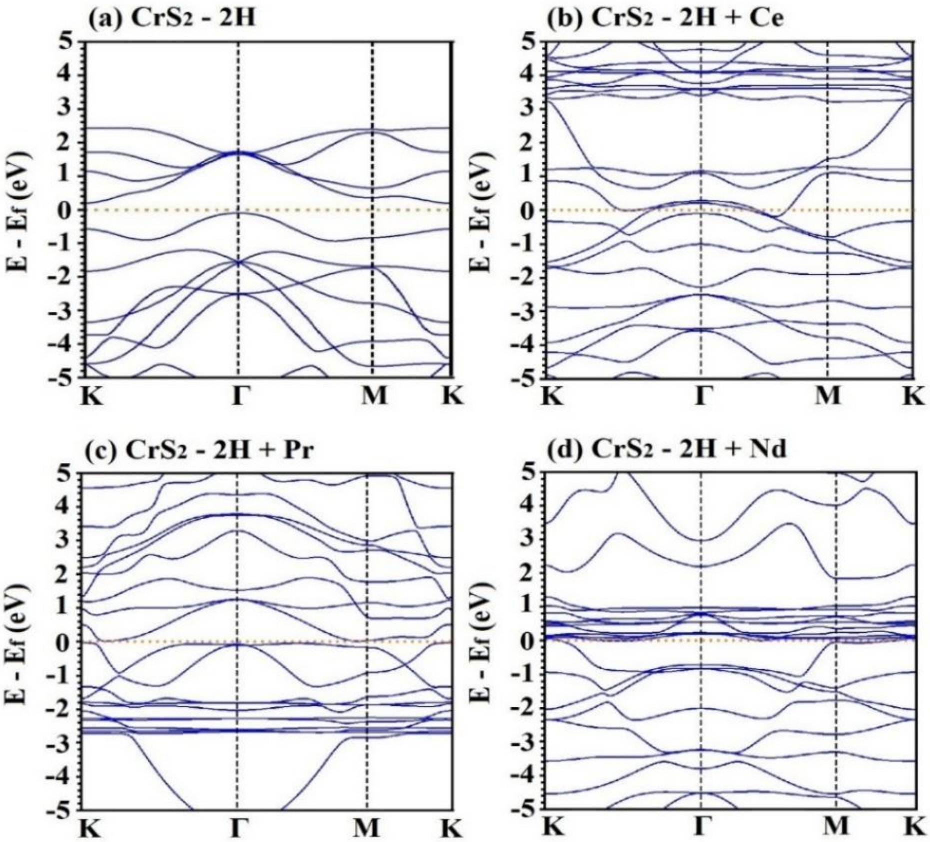

Figure 7: Band structure of (a) hexagonal phase of CrS_2 monolayer in the absence of lanthanide atoms, (b) hexagonal phase of CrS_2 monolayer in the presence of Ce atom, (c) hexagonal phase of CrS_2 monolayer in the presence of Pr atom, and (d) hexagonal phase of CrS_2 monolayer in the presence of Nd atom. The Fermi level is marked with an orange dashed dot at the zero point

To facilitate comparison, the Fermi level of all structures at the zero point is marked with an orange dotted line. According to the band structure diagrams, it is evident that the octahedral phase of CrX_2 (where X=S, Se) structures exhibits metallic behavior (MB), with several bands intersecting the Fermi level. However, the hexagonal phase of these structures demonstrates semiconducting behavior and possesses a band gap. Specifically, the hexagonal CrS_2 and $CrSe_2$ monolayers have band gaps of 0.30 eV and 0.44 eV, respectively. The previous studies also support that hexagonal and octahedral CrX_2 structures exhibit semiconducting and metallic behavior, respectively. The electronic configurations for the Cr atom are [Ar] $3d^5$ $4s^1$. The d orbital dictates the electronic behavior of the material. If the d orbital is completely full or empty, the TMDs exhibit semiconducting characteristics, whereas if the d orbital is partially occupied, the TMDs exhibit metallic behavior. The crystal symmetry, i.e. the polymorphic phase, significantly influences the energy of the d bands, resulting in different electronic properties depending on the polymorphic phase. For instance, in this study, CrX_2 is metallic in the 1T phase but semiconductor in the 2H phase. The bandgap values of the examined structures and the reported band gap sizes from previous are provided in Table 2 [11-13]. There is a discrepancy between the results of this research and other studies, which is attributed to the type of exchange-correlation functional. The exchange-correlation functional used in this study is GGA-PBE approximation, whereas most other articles employ different functionals such as Heyd–Scuseria–Ernzerhof functional (HSE06). In the first principle methods based on density functional theory, the use of local exchange-correlation functionals (such as the LDA approximation) and semi-local (such as the generalized gradient approximation GGA-PBE) in calculating the band gap of semiconductors results in the gap being obtained to a much lesser extent than the experimental value. The use of hybrid functionals such as PBE0 and HSE06, in which a non-local Hartree-Fock exchange is combined with an LDA or GGA functional, reduces the self-interaction energy error and leads to more accurate values of the band gap, but the computational cost of using these functionals is very high [37]. For instance, Kaiyun Chen *et al.* [9] calculated and compared the band structure using GGA-PBE and HSE06 methods. Their results show that the band gap obtained by the GGA-PBE and HSE06 methods is 0.3734eV and 0.7642eV, respectively, which is consistent with the results of this study based on the GGA-PBE method.

For the hexagonal phase of CrS2 in the presence of lanthanide atoms (L = Ce, Pr, and Nd), several bands intersect the Fermi level, indicating metallic behavior. In the presence of Ce atoms, these bands are densely concentrated in the conduction band (ranging from +3 eV to +5 eV), attributed to their 4f shells. The electronic configurations for Ce, Nd, and Pr are [Xe]$4f^1$ $5d^1$ $6s^2$, [Xe]$4f^4$ $5d^0$ $6s^2$, and [Xe]$4f^3$ $5d^0$ $6s^2$, respectively. With Nd atoms, these bands are situated around the Fermi level, while for Pr atoms, they are located in the valence band. In the octahedral phase, only with Ce atoms does the structure exhibit semiconducting behavior with a band gap of 0.42 eV, while in the presence of Nd and Pr atoms, it displays metallic behavior. systems.

Similar behavior was observed by Ouma *et al.* [38]. They studied electronic, magnetic and optical properties of lanthanide substitutional doping on the MoS_2 monolayer. They reported that the d and f orbitals of the dopants play a key role in determining the electronic properties of the doped systems. The spin asymmetry of the d and f states near the Fermi level gives rise to a non-zero band gap in Ce doped Focusing on the case of d and f donor states show that these states result from the d_{z^2} and $f_{x^3-3xy^2}$ orbital in the case of Ce doping. Likewise, researchers reported that introducing transition metal (TM) in 2D system is an effective route to modulate its electronic properties. TM doping in MoS_2 sheet provides a new strategy to obtain diluted magnetic semiconductors [39].

The accumulation of bands in this case is predominantly observed for the Pr atom around the Fermi level. Both the hexagonal and octahedral phases of $CrSe_2$ demonstrate metallic behavior in the presence of lanthanide atoms (L = Ce, Pr, and Nd). The band accumulation pattern in the hexagonal phase of $CrSe_2$ mirrors that of CrS_2-2H. However, in the octahedral phase of $CrSe_2$, band accumulation in the presence of Ce and Nd atoms occurs in the conduction band, whereas for Pr atoms, it is observed in the valence band and close to the Fermi level.

Table 2: Band gap of hexagonal (2H) and octahedral (1T) phases of CrX_2 (where X=S, Se) structures after relaxation in the presence and absence of lanthanide atoms (L=Ce, Pr, and Nd)

Structure		Band gap without spin polarization (eV)	Band gap with spin polarization (eV)
CrS_2 - 2H	pure	0.30 1.35 [9] 0.970 [41] 0.604 [11]	Up: MB Down: MB
	+Ce	MB	Up: MB Down: MB
	+Pr	MB	Up: MB Down: 0.50
	+Nd	MB	Up: MB Down: MB
CrS_2 - 1T	Pure	MB 0.0 [14]	Up: MB Down: MB
	+Ce	0.42	Up: MB Down: 0.40
	+Pr	MB	Up: MB Down: MB
	+Nd	MB	Up: MB Down: MB
$CrSe_2$ - 2H	Pure	0.44 0.789 [41] 0.589 [11]	Up: MB Down: MB
	+Ce	MB	Up: MB Down: MB
	+Pr	MB	Up: MB Down: 0.48
	+Nd	MB	Up: MB Down: MB
$CrSe_2$ - 1T	Pure	MB	Up: MB Down: MB
	+Ce	MB	Up: MB Down: MB
	+Pr	MB	Up: MB Down: MB
	+Nd	MB	Up: MB Down: MB

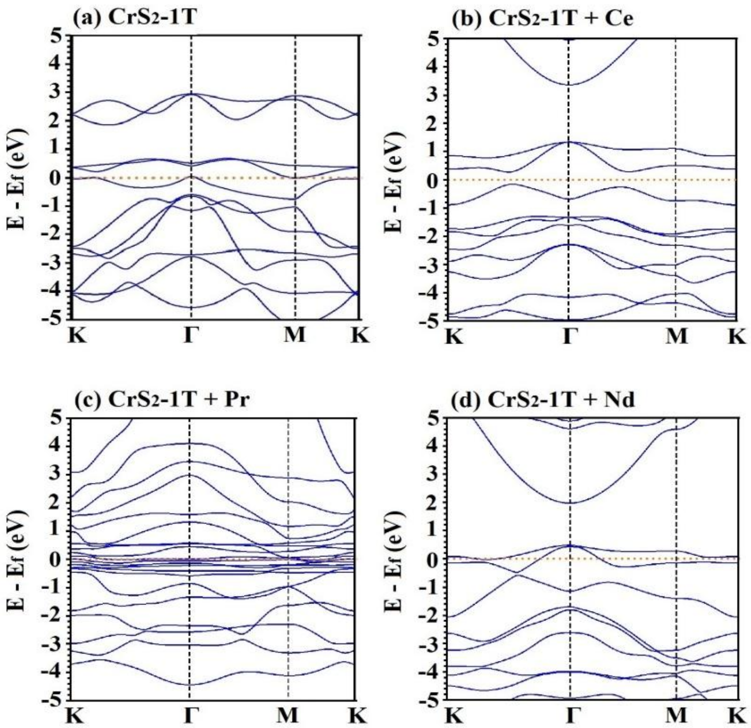

Figure 8: Band structure of (a) octahedral phase of CrS_2 monolayer in the absence of lanthanide atoms, (b) octahedral phase of CrS_2 monolayer in the presence of Ce atom, (c) octahedral phase of CrS_2 monolayer in the presence of Pr atom, and (d) octahedral phase of CrS_2 monolayer in the presence of Nd atom. The Fermi level is marked with an orange dashed dot at the zero point

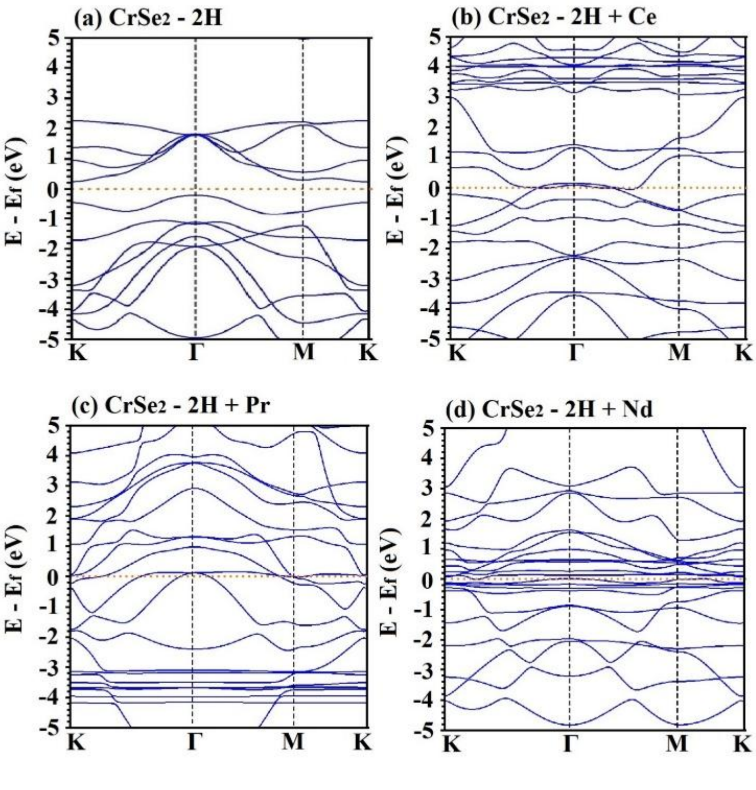

Figure 9: Band structure of (a) hexagonal phase of $CrSe_2$ monolayer in the absence of lanthanide atoms, (b) hexagonal phase of $CrSe_2$ monolayer in the presence of Ce atom, (c) hexagonal phase of $CrSe_2$ monolayer in the presence of Pr atom, and (d) hexagonal phase of $CrSe_2$ monolayer in the presence of Nd atom. The Fermi level is marked with an orange dashed dot at the zero point

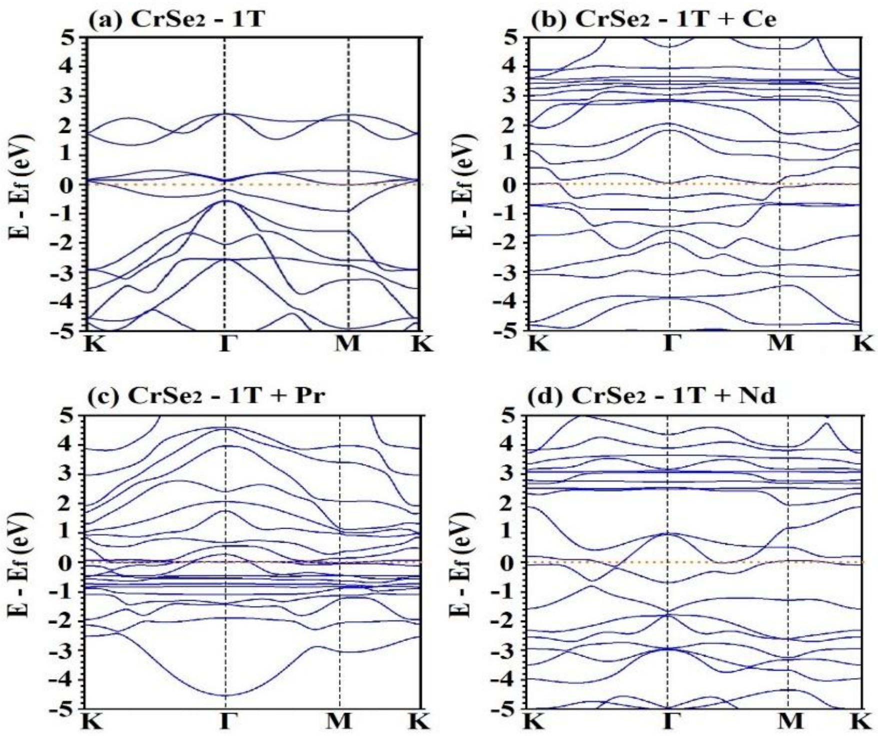

Figure 10: Band structure of (a) octahedral phase of $CrSe_2$ monolayer in the absence of lanthanide atoms, (b) octahedral phase of $CrSe_2$ monolayer in the presence of Ce atom, (c) octahedral phase of $CrSe_2$ monolayer in the presence of Pr atom, and (d) octahedral phase of $CrSe_2$ monolayer in the presence of Nd atom. The Fermi level is marked with an orange dashed dot at the zero point

Band Structure of CrX_2 Monolayers in the Presence and Absence of Lanthanide Atoms Considering Spin Polarization Effect

The band structure of CrS_2-2H, CrS_2-1T, $CrSe_2$-2H, and $CrSe_2$-1T monolayers both with and without lanthanide atoms (L=Ce, Pr, and Nd) for up and down spins are demonstrated in Figures 11-14. The Fermi level of all structures is at the zero point and marked with a blue dotted line. Up spin is depicted in black, and down spin is illustrated in red line. Upon examining the band structure of CrS_2-2H, CrS_2-1T, $CrSe_2$-2H, and $CrSe_2$-1T monolayers while concerning spin effects, it is observed that the hexagonal CrS_2 structure, only with Pr atoms and for down spin, exhibits a direct band gap of 0.50 eV, indicating half metal behavior. In all other states, it displays metallic behavior.

A half-metal material is metallic in one spin channel and exhibits semiconductor or insulator behavior in the opposite channel and are essential for spintronics applications where one needs to read, write, store, and transfer spin-data. The field of spintronics is based upon the use of the direction of spin of electrons rather than their charge. Zhicui Wang *et al.* [40] were designed and examined MX_2 (M = Cr, Mn; X = Se, Te) magnetic material with a square lattice through first-principle calculations. Their results show that Ferromagnetic half-metal materials are considered as crucial materials for the spintronic devices due to the fully spin-polarized carrier transport.

In the case of the octahedral CrS_2 monolayer with Ce atoms for down spin, an indirect band gap of 0.40 eV can be observed, representing the half-metal behavior of this structure, while the rest exhibit metallic behavior. Similarly, hexagonal $CrSe_2$ displays a band gap of 0.48 eV with Pr atoms for down spin, indicating half-metal behavior, whereas other structures exhibit metallic behavior. However, the octahedral $CrSe_2$ behaves metallically with lanthanide atoms, considering spin effects. The band gap value of the studied structures both with and without lanthanide atoms, considering up and down spin, is reported in Table 2. A comparison of the band structure in Figures 11-14 reveals asymmetry between up and down spins in all these structures, indicating their magnetic nature. The band structure of CrS_2-2H and $CrSe_2$-2H with and without lanthanide atoms exhibits similar patterns, with band accumulation near the Fermi level observed only for Pr and Nd atoms. This pattern is also evident in the octahedral phase of CrS_2 and $CrSe_2$.

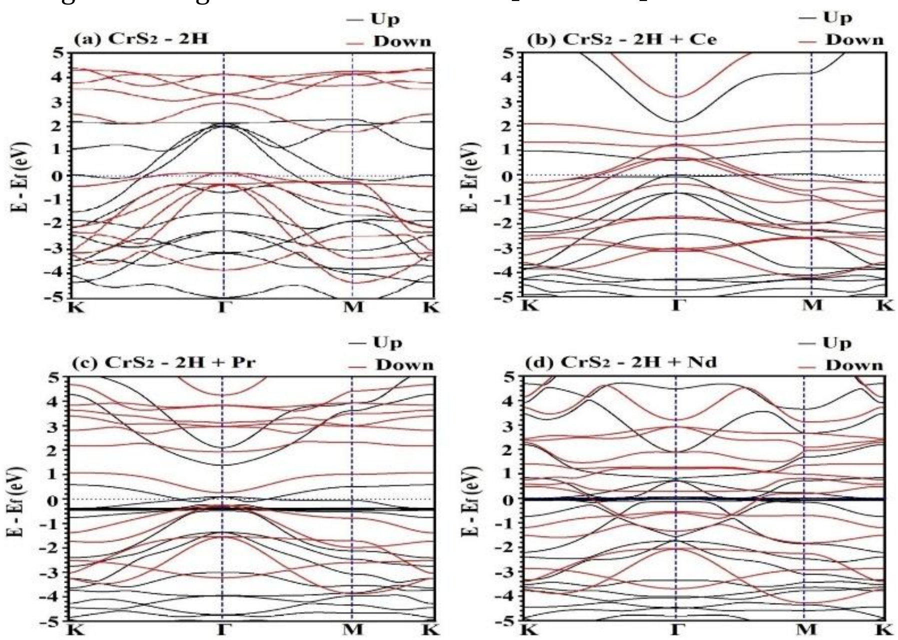

Figure 11: Band structure of (a) hexagonal phase of CrS_2 monolayer in the absence of lanthanide atoms, (b) hexagonal phase of CrS_2 monolayer in the presence of Ce atom, (c) hexagonal phase of CrS_2 monolayer in the presence of Pr atom, and (d) hexagonal phase of CrS_2 monolayer in the presence of Nd atom. The Fermi level is marked with a dashed blue dot at the zero point. Up spin is marked in black and down spin is marked in red

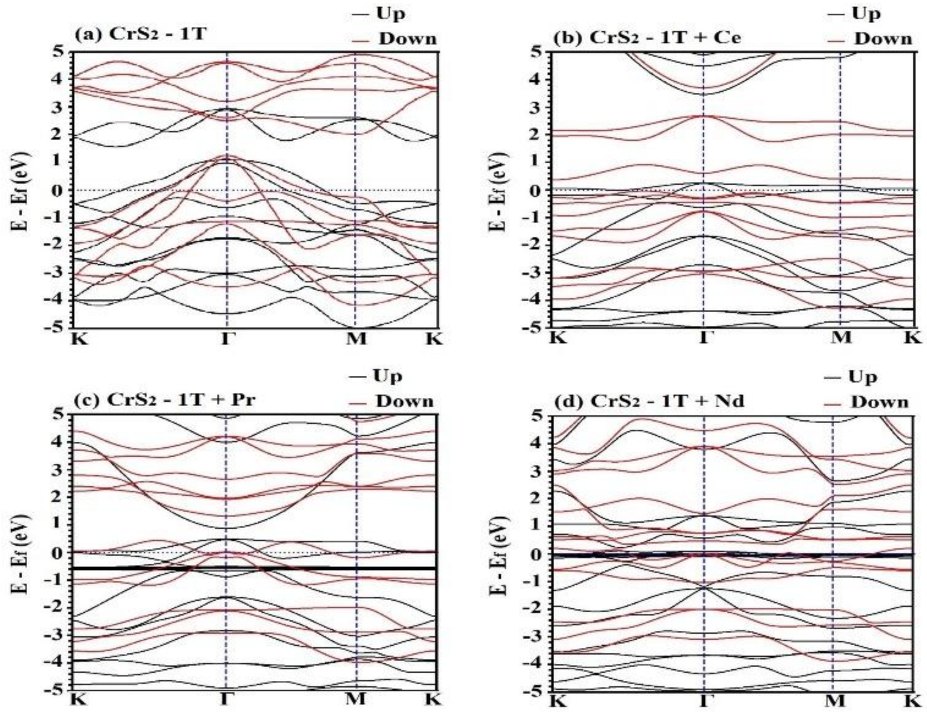

Figure 12: Band structure of (a) octahedral phase of CrS_2 monolayer in the absence of lanthanide atoms, (b) octahedral phase of CrS_2 monolayer in the presence of Ce atom, (c) octahedral phase of CrS_2 monolayer in the presence of Pr atom, and (d) octahedral phase of CrS_2 monolayer in the presence of Nd atom. The Fermi level is marked with a dashed blue dot at the zero point. Up spin is marked in black and down spin is marked in red

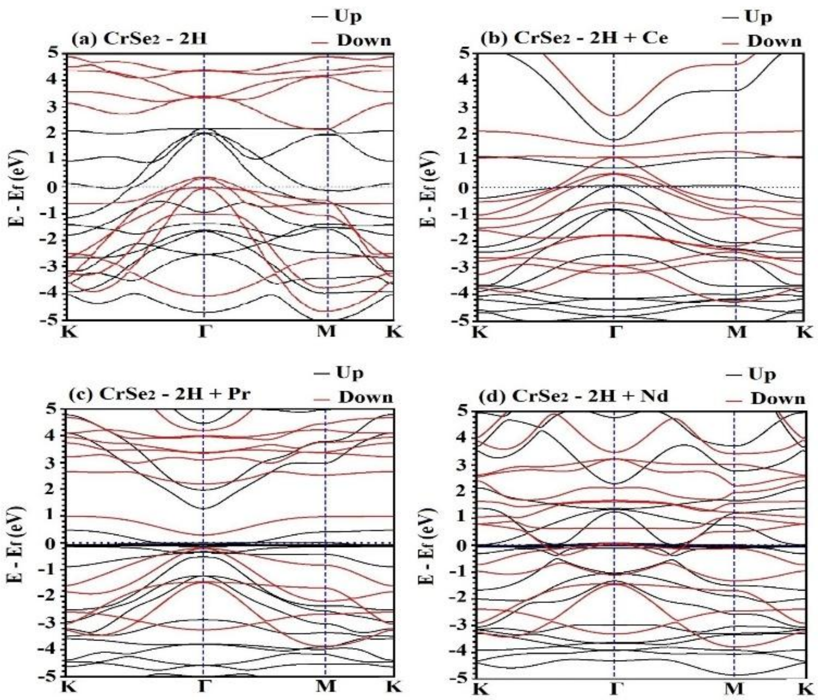

Figure 13: Band structure of (a) hexagonal phase of $CrSe_2$ monolayer in the absence of lanthanide atoms, (b) hexagonal phase of $CrSe_2$ monolayer in the presence of Ce atom, (c) hexagonal phase of $CrSe_2$ monolayer in the presence of Pr atom, and (d) hexagonal phase of $CrSe_2$ monolayer in the presence of Nd atom. The Fermi level is marked with a dashed blue dot at the zero point. Up spin is marked in black and down spin is marked in red

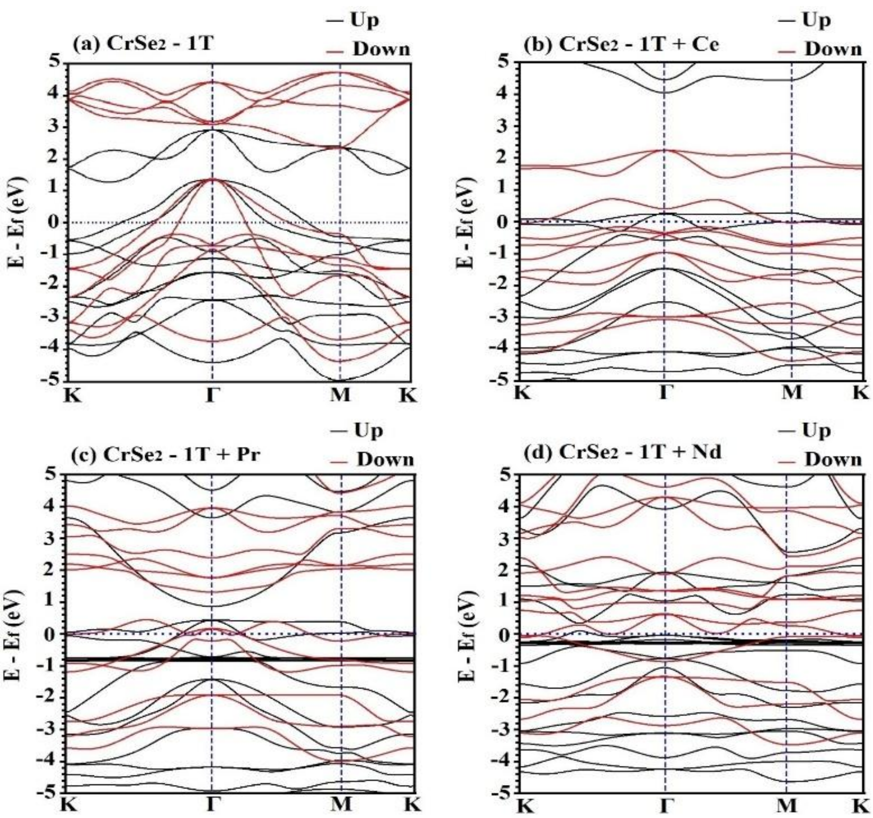

Figure 14: Band structure of (a) octahedral phase of $CrSe_2$ monolayer in the absence of lanthanide atoms, (b) octahedral phase of $CrSe_2$ monolayer in the presence of Ce atom, (c) octahedral phase of $CrSe_2$ monolayer in the presence of Pr atom, and (d) octahedral phase of $CrSe_2$ monolayer in the presence of Nd atom. The Fermi level is marked with a dashed blue dot at the zero point. Up spin is marked in black and down spin is marked in red

To investigate the magnetic properties of the CrX_2 monolayer (X=S, Se) with and without lanthanide atoms (L= Ce, Pr, and Nd), the magnetic moment of these structures was calculated and presented in Table 3. The results showed that the magnetic moment of all these structures is non-zero, signifying their magnetic ground state. Taking into account the electronic configuration of lanthanide atoms, it was observed that in Ce, Pr, and Nd atoms, the outermost orbital layer is 4f, which remains partially filled, resulting in the formation of a magnetic ground state. In addition, with the presence of lanthanides and increasing the atomic number of lanthanides, the magnetic moment rises.

Table 3: Magnetic moment value of CrX_2 (where X=S, Se) monolayer with and without lanthanide atoms (L= Ce, Pr, and Nd)

STRUCTURE	CRS_2-2H				CRS_2-1T				$CRSE_2$-2H				$CRSE_2$-1T			
	Pure	+Ce	+Pr	+Nd	Pure	+Ce	+Pr	+Nd	Pure	+Ce	+Pr	+Nd	Pure	+Ce	+Pr	+ND
M (μB)	2.00	5.39	6.69	7.25	2.21	5.27	6.43	7.14	2.14	5.58	6.98	7.39	2.45	5.23	6.43	7.18

Conclusion

This study examined the structural and electronic properties of CrX_2 (X=S, Se) monolayers both with and without lanthanide atoms (L= Ce, Pr, and Nd). The Quantum Espresso computing code, which is rooted in the density functional theory approach, was employed to calculate the structural and electronic properties through GGA-PBE approximation. The effect of dopant atoms on the electronic band structure was also studied and analyzed. In this research, we examined two additional stable phases: 2H and 1T. The 2H phase can be converted to the 1T phase by sliding the top layer (X atoms) to the hexagon centers.

Structural results show that with the inclusion of lanthanide atoms, the stability of the structures increased compared to the pure state, and the total energy became more negative. With the increase in atomic number of lanthanides doped into the structure increased, the total energy became more negative, enhancing the structure's stability. Moreover, increasing the atomic number of lanthanides led to longer Cr-X and L-X bond lengths while reducing X-Cr-X and X-L-X bond angles.

Results from the band structure show that hexagonal/octahedral phases of CrX_2 (where X=S, Se) structures displaying semiconducting/metallic behavior. In particular, the hexagonal CrS_2 and $CrSe_2$ monolayers have band gaps of 0.30 eV and 0.44 eV, respectively. In the hexagonal phase of CrS_2 in the presence of lanthanide atoms, several bands cut the Fermi level, indicating metallic behavior. In contrast, in the octahedral phase, only with Ce atoms does the structure exhibit semiconducting behavior with a band gap of 0.42 eV, while in the presence of Nd and Pr atoms, it displays metallic behavior. Similarly, the hexagonal and octahedral phases of $CrSe_2$ indicate metallic behavior with lanthanide atoms.

Taking into account spin-polarized effects, CrS_2-2H+Pr, CrS_2-1T+Ce, and $CrSe_2$-2H+Pr exhibit a band gap for the down spin, indicating half-metal behavior. Given that half-metal materials offer the possibility of unprecedented magnetoresistance, there is huge potential for device applications. More interestingly, we found that the doping with lanthanide atom could turn CrS_2 and $CrSe_2$ into spin-down half metals. Such a unique feature enables the designing of spintronic devices using a monolayer of CrS_2/$CrSe_2$ crystal, which poses a challenge in the miniaturization of spintronic devices.

References

[1]. Zhao B., Shen D., Zhang Z., Lu P., Hossain M., Li J., Li B., Duan X., 2d metallic transition-metal dichalcogenides: Structures, synthesis, properties, and applications, *Advanced Functional Materials*, 2021, **31**:2105132 [Crossref], [Google Scholar], [Publisher]

[2]. LV H., Lu W., Shao D., Liu Y., Sun Y., Strain-controlled switch between ferromagnetism and antiferromagnetism in 1 T-Cr X 2 (X= Se, Te) monolayers. *Physical Review B*, 2015, **92**:214419 [Crossref], [Google Scholar], [Publisher]

[3]. Zhang X., Jin Z., Wang L., Hachtel J.A., Villarreal E., Wang Z., Ha T., Nakanishi Y., Tiwary C.S., Lai J., Low contact barrier in 2H/1T′ MoTe2 in-plane heterostructure synthesized by chemical vapor deposition, *ACS Applied Materials & Interfaces*, 2019, **11**:12777 [Crossref], [Google Scholar], [Publisher]

[4]. Pereira V.M., Castro Neto A., Strain engineering of graphene's electronic structure, *Physical Review Letters*, 2009, **103**:046801 [Crossref], [Google Scholar], [Publisher]

[5]. Wang D., Zhang X., Bao S., Zhang Z., Fei H., Wu Z., Phase engineering of a multiphasic 1T/2H MoS 2 catalyst for highly efficient hydrogen evolution, *Journal of Materials Chemistry A*, 2017, **5**:2681 [Crossref], [Google Scholar], [Publisher]

[6].a) Tajik S., Garkani Nejad F., Zaimbashi R., Beitollai H., Voltammetric Sensor for Acyclovir Determination Based on $MoSe_2$/rGO Nanocomposite Modified Electrode, *Chemical Methodologies*, 2024, **8**:316 [Crossref], [Google Scholar], [Publisher]

b) Liu Z., Ma L., Shi G., Zhou W., Gong Y., Lei S., Yang X., Zhang J., Yu J., Hackenberg K.P., In-plane heterostructures of graphene and hexagonal boron nitride with controlled domain sizes, *Nature Nanotechnology*, 2013, **8**:119 [Crossref], [Google Scholar], [Publisher]

[7]. Kappera R., Voiry D., Yalcin S.E., Branch B., Gupta G., Mohite A.D., Chhowalla M., Phase-engineered low-resistance contacts for ultrathin MoS2 transistors, *Nature Materials*, 2014, **13**:1128 [Crossref], [Google Scholar], [Publisher]

[8]. a) Samuel H.S., Nweke-Maraizu U., Etim E.E. E. Unleashing the Potential of Machine Learning in Chalcogen Bonding Research, *Eurasian Journal of Science and Technology*, 2024, **4**:133 [Crossref], [Google Scholar], [Publisher]

b) Chen K., Wan X., Wen J., Xie W., Kang Z., Zeng X., Chen H., Xu J.B., Electronic properties of MoS2–WS2 heterostructures synthesized with two-step lateral epitaxial strategy. *ACS Nano*, 2015, **9**:9868 [Crossref], [Google Scholar], [Publisher]

[9]. Chen K., Deng J., Yan Y., Shi Q., Chang T., Ding X., Sun J., Yang S., Liu J.Z., Diverse electronic and magnetic properties of CrS2 enabling strain-controlled 2d lateral heterostructure spintronic devices, *Npj Computational Materials*, 2021, **7**:79 [Crossref], [Google Scholar], [Publisher]

[10]. Hasan M., Ta H.Q., Ullah S., Yang X., Luo J., Bachmatiuk A., Gemming T., Trzebicka B., Mahmood A., Zeng M., Crystal structure, synthesis and characterization of different chromium-based two-dimensional compounds, *Arabian Journal of Chemistry*, 2023, **16**:104973 [Crossref], [Google Scholar], [Publisher]

[11]. Sun X., Wang Z., Ab initio study of adsorption and diffusion of lithium on transition metal dichalcogenide monolayers, *Beilstein Journal of Nanotechnology*, 2017, **8**:2711 [Crossref], [Google Scholar], [Publisher]

[12]. Bastos C.M., Besse R., Da Silva J.L., Sipahi G.M., Ab initio investigation of structural stability and exfoliation energies in transition metal dichalcogenides based on Ti-, V-, and Mo-group elements. *Physical Review Materials*, 2019, **3**:044002 [Crossref], [Google Scholar], [Publisher]

[13]. Wang C., Zhou X., Pan Y., Qiao J., Kong X., Kaun C.C., Ji W., Layer and doping tunable ferromagnetic order in two-dimensional Cr S 2 layers, *Physical Review B*, 2018, **97**:245409 [Crossref], [Google Scholar], [Publisher]

[14]. Korotaev E., Syrokvashin M., Filatova I.Y., Kalinkin A., Sotnikov A., Valence band structure and charge distribution in the layered lanthanide-doped cucr0. 99ln0. 01s2 (Ln= La, Ce) solid solutions, *Scientific Reports*, 2021, **11**:18934 [Crossref], [Google Scholar], [Publisher]

[15]. Wolf S., Awschalom D., Buhrman R., Daughton J., von Molnár V.S., Roukes M., Chtchelkanova A.Y., Treger D., Spintronics: A spin-based electronics vision for the future, *Science*, 2001, **294**:1488 [Crossref], [Google Scholar], [Publisher]

[16]. a) Shah H., Afzal S., Usman M., Shahzad K., Ikhioya I.L., Impact of Annealing Temperature on Lanthanum Erbium Telluride ($La_{0.1}Er_{0.}2Te_{0.2}$) Nanoparticles Synthesized via Hydrothermal Approach', *Advanced Journal of Chemistry, Section*

A, 2023, **6**:342 [Crossref], [Google Scholar], [Publisher]

b) Hirohata A., Takanashi K., Future perspectives for spintronic devices. *Journal of Physics D: Applied Physics*, 2014, **47**:193001 [Crossref], [Google Scholar], [Publisher]

[17]. Han W., Perspectives for spintronics in 2D materials. *Apl Materials*, 2016, **4:**032401 [Crossref], [Google Scholar], [Publisher]

[18]. Han W., Kawakami R.K., Gmitra M., Fabian J., Graphene spintronics, *Nature Nanotechnology*, 2014, **9**:794 [Crossref], [Google Scholar], [Publisher]

[19]. Baibich M.N., Broto J.M., Fert A., Van Dau F.N., Petroff F., Etienne P., Creuzet G., Friederich A Chazelas, J., Giant magnetoresistance of (001)Fe/(001)Cr magnetic superlattices. *Physical Review Letters*, 1988, **61**:2472 [Crossref], [Google Scholar], [Publisher]

[20] .Moodera J.S., Kinder L.R., Wong T.M., Meservey R., Large magnetoresistance at room temperature in ferromagnetic thin film tunnel junctions, *Physical Review Letters*, 1995, **74**:3273 [Crossref], [Google Scholar], [Publisher]

[21]. Fan Y., Upadhyaya P., Kou X., Lang M., Takei S., Wang Z., Tang J., He L., Chang L.-T., Montazeri M., Magnetization switching through giant spin–orbit torque in a magnetically doped topological insulator heterostructure, *Nature Materials*, 2014, **13**:699 [Crossref], [Google Scholar], [Publisher]

[22]. Zhang X., Teng S.Y., Loy A.C.M., How B.S., Leong W.D., Tao X., Transition metal dichalcogenides for the application of pollution reduction: A review, *Nanomaterials*, 2020, **10**:1012 [Crossref], [Google Scholar], [Publisher]

[23]. Chhowalla M., H.S. Shin, G. Eda, L.J. Li, k. P. Loh and h. Zhang, *Nat. Chem*, 2013, **5**:263 [Crossref], [Google Scholar], [Publisher]

[24]. Mak K.F., McGill K.L., Park J., McEuen P.L., The valley hall effect in MoS2 transistors, *Science*, 2014, **344**:1489 [Crossref], [Google Scholar], [Publisher]

[25]. Barja S., Wickenburg S., Liu Z.F., Zhang Y., Ryu H., Ugeda M.M., Hussain Z., Shen Z.X., Mo S.K., Wong E., Charge density wave order in 1d mirror twin boundaries of single-layer MoSe 2, *Nature Physics*, 2016, **12**:751 [Crossref], [Google Scholar], [Publisher]

[26]. Lin J., Pantelides S.T., Zhou W., Vacancy-induced formation and growth of inversion domains in transition-metal dichalcogenide monolayer, *Acs Nano*, 2015, **9**:5189 [Crossref], [Google Scholar], [Publisher]

[27]. Liu H., Jiao L., Yang F., Cai Y., Wu X., Ho W., Gao C., Jia J., Wang N., Fan H., Dense network of one-dimensional midgap metallic modes in monolayer MoSe 2 and their spatial undulations, *Physical Review Letters*, 2014, **113**:066105 [Crossref], [Google Scholar], [Publisher]

[28]. Giannozzi P., Baroni S., Bonini N., Calandra M., Car R., Cavazzoni C., Ceresoli D., Chiarotti G.L., Cococcioni M., Dabo I., Quantum espresso: A modular and open-source software project for quantumsimulations of materials, *Journal of Physics: Condensed Matter*, 2009, **21**:395502 [Crossref], [Google Scholar], [Publisher]

[29]. Do T.N., Nguyen C., Tan L.V., Idrees M., Amin B., Hieu N.V., Hoai N.T., Hoa L.T., Hieu N.N., Phuc H.V., Effects of la and Ce doping on electronic structure and optical properties of janus MoSSe monolayer, *Superlattices and Microstructures*, 2021, **151**:106841 [Crossref], [Google Scholar], [Publisher]

[30]. Ikram M., Ilyas B., Haider A., Haider J., Ul-Hamid A., Shahzadi A., Goumri-Said S., Kanoun M.B., Nabgan W., Mahmood A., Fabrication of la-doped mos2 nanosheets with tuned bandgap for dye degradation and antimicrobial activities, experimental and computational investigations, *Advanced Materials Interfaces*, 2023, **10**:2202404 [Crossref], [Google Scholar], [Publisher]

[31]. Gange J., Yuqi J., Xiang G., Zhao D., First principles study of rare earth elements (La, Eu, Ho) doped monolayer WSe_2. *Journal of Functional Materials/Gongneng Cailiao*, 2024, **55**:2155 [Crossref], [Google Scholar], [Publisher]

[32]. Giannozzi P., Andreussi O., Brumme T., Bunau O., Nardelli M.B., Calandra M., Car R., Cavazzoni C., Ceresoli D., Cococcioni M., Advanced capabilities for materials modelling with quantum espresso, *Journal of Physics: Condensed Matter*, 2017, **29**:465901 [Crossref], [Google Scholar], [Publisher]

[33]. Paasch G., Übensee H., A modified local density approximation. Electron density in inversion layers, *Physica Status Solidi (b)*, 1982, **113**:165 [Crossref], [Google Scholar], [Publisher]

[34]. Habib M.R., Wang S., Wang W., Xiao H., Obaidulla S.M., Gayen A., Khan Y., Chen H., Xu M., Electronic properties of polymorphic two-dimensional layered chromium disulphide, *Nanoscale*, 2019, **11**:20123 [Crossref], [Google Scholar], [Publisher]

[35]. Awate S.S., Xu K., Liang J., Katz B., Muzzio R., Crespi V.H., Katoch J., Fullerton-Shirey S.K., Strain-induced 2H to 1T′ phase transition in suspended MoTe2 using electric double layer gating, *ACS Nano*, 2023, **17**:22388 [Crossref], [Google Scholar], [Publisher]

[36]. Jin Q., Liu N., Chen B., Mei D., Mechanisms of semiconducting 2H to metallic 1T phase transition in two-dimensional MoS2 nanosheets, *The Journal of Physical Chemistry C*, 2018, **122**:28215 [Crossref], [Google Scholar], [Publisher]

[37]. Eivari H.A., Hafizi R., Mechanical properties of two-dimensional sheets of Tio 2: A DFT study, *The European Physical Journal Plus*, 2022, **137**:1128 [Crossref], [Google Scholar], [Publisher]

[38]. Ouma C.N., Singh S., Obodo K.O., Amolo G.O., Romero A.H., Controlling the magnetic and optical responses of a MoS_2 monolayer by lanthanide substitutional doping: A first-principles study, *Physical Chemistry Chemical Physics*, 2017, **19**:25555 [Crossref], [Google Scholar], [Publisher]

[39]. Chen Z., He J., Zhou P., Na J., Sun L., Strain control of the electronic structures, magnetic states, and magnetic anisotropy of Fe doped single-layer MoS2, *Computational Materials Science*, 2015, **110**:102 [Crossref], [Google Scholar], [Publisher]

[40] Wang Z., Zhang M., Ge Y., Wan W., Liu Y., Monolayer MX_2 (M= Cr, Mn; X= Se, Te) with a square lattice: A ferromagnetic half-metal with high curie temperature, *Results in Physics*, 2023, **51**:106687 [Crossref], [Google Scholar], [Publisher]

[41]. Abdullah S.A., Roknabadi M.R., Behdani M., Ab initio investigation of structural, electronic and magnetic properties of oh-functionalized monolayer CrX_2 (X= S, Se, Te), *Journal of Theoretical and Applied Physics*, 2024, **18**:1 [Crossref], [Google Scholar], [Publisher]

Use your device to scan and read the article online

HOW TO CITE THIS ARTICLE
M.K.J. Almuttwaki, M. Rezaee Roknabadi, M. Modarresi, Theoretical study of the effect of phase transition on the structural and electronic properties of lanthanide-doped chromium chalcogenide monolayers. *Chem. Methodol.*, 2025, 9(8) 643-661
DOI: https:// 10.48309/CHEMM.2025.506714.1905
URL: https://www.chemmethod.com/article_220416.html